



On-site quantitative Hg^{2+} measurements based on selective and sensitive fluorescence biosensor and miniaturized smartphone fluorescence microscope

Yanke Shan^{a,1}, Bin Wang^{a,1}, Huachuan Huang^{b,1}, Dan Jian^c, Xuping Wu^d, Liang Xue^e, Shouyu Wang^{a,c,*}, Fei Liu^{a,*}

^a Joint International Research Laboratory of Animal Health and Food Safety of Ministry of Education & Single Molecule Nanometry Laboratory (Sinmolab), Nanjing Agricultural University, Nanjing, Jiangsu, 210095, China

^b School of Manufacturing Science and Engineering, Southwest University of Science and Technology, Mianyang, Sichuan 621010, China

^c Computational Optics Laboratory, School of Science, Jiangnan University, Wuxi, Jiangsu 214122, China

^d The Second Hospital of Nanjing Affiliated to Southeast University, Nanjing, Jiangsu 210003, China

^e College of Electronics and Information Engineering, Shanghai University of Electric Power, Shanghai 200090, China

ARTICLE INFO

Keywords:

Smart Hg^{2+} detection method
Thymine- Hg^{2+} -thymine coordination chemistry
Smartphone fluorescence microscope
Quantitative Hg^{2+} measurements
On-site detection

ABSTRACT

Mercury is a bio-accumulative and toxic pollutant causing severe damages to human health and environment. Since Hg^{2+} is the most stable form of mercury, selective and sensitive Hg^{2+} detection is required. Though classical approaches can realize accurate Hg^{2+} detection, the complicated instruments and the time-consuming operations inevitably limit their on-site applications. Here, we design a smart Hg^{2+} detection approach using the fluorescence biosensor, the smartphone fluorescence microscope and the smartphone application for Hg^{2+} on-site detection. Based on the thymine- Hg^{2+} -thymine coordination chemistry, a selective and sensitive fluorescence biosensor is designed for capturing Hg^{2+} in aqueous solution; besides, a miniaturized smartphone fluorescence microscope for fluorescence signal collection and an image processing application for quantitative Hg^{2+} measurements are constructed. A highly specific detection of Hg^{2+} with a linear relation between 1 nM and 1 μM with a limit of detection of 1 nM is obtained using the smart Hg^{2+} detection approach. Considering it can realize selective and sensitive quantitative Hg^{2+} measurements in high precision with simple operations and cost-effective system, it is believed the proposed smart Hg^{2+} detection approach owns great potentials in Hg^{2+} detection for routine uses at home and in the field.

1. Introduction

Mercury is a bio-accumulative and highly toxic environmental pollutant that causes severe damages to the nerve system, heart, kidney and many other organs even at low concentrations (Boening, 2000; Hoyle and Handy, 2005). It will invade the human body through the respiratory and digestive tracts as well as the skin (Baughman, 2006). Natural processes and human activities, such as coal and gold mining, wood pulping, solid waste incineration, fossil fuel combustion, and chemical manufacturing, may cause mercury released into the environment (Nolan and Lippard, 2008). Mercury exists in various forms, including metal oxide, metal ion and organic complexes, etc. Among them, Hg^{2+} is the most stable form (Li et al., 2010), and even trace

amount of Hg^{2+} contamination in drinking water or other natural water resources could threaten human health (Yang et al., 2014), therefore selective and sensitive Hg^{2+} detection in aqueous solution is required to prevent poisoning of Hg^{2+} .

Recently there are many effects on developing various nano- and bio-sensing approaches (Ai, 2014; Chandra, 2016; Thompson, 2005) for Hg^{2+} detection in aqueous solution such as tap water, river water or PBS buffer, etc. (Chen et al., 2014, 2015; Jiang et al., 2014; Wei et al., 2014; Wu et al., 2016; Zhang et al., 2015). Classical methods for Hg^{2+} detection include inductively coupled plasma mass spectroscopy (Li et al., 2006; Santos et al., 2012), cold vapor atomic fluorescence/absorption spectroscopy (Ai et al., 2013; Kunkel and Manahan, 1973; Shah et al., 2010) and atomic absorption/emission spectroscopy (Han

* Corresponding authors at: Joint International Research Laboratory of Animal Health and Food Safety of Ministry of Education & Single Molecule Nanometry Laboratory (Sinmolab), Nanjing Agricultural University, Nanjing, Jiangsu 210095, China.

E-mail addresses: shouyu@jiangnan.edu.cn (S. Wang), feiliu24@njau.edu.cn (F. Liu).

¹ These authors contributed equally to this work.

<https://doi.org/10.1016/j.bios.2019.02.062>

Received 5 November 2018; Received in revised form 16 February 2019; Accepted 25 February 2019

Available online 07 March 2019

0956-5663/© 2019 Elsevier B.V. All rights reserved.

et al., 2006). These methods are very sensitive and selective, but require complicated instruments, time-consuming sample pretreatment and professional operators. To solve these problems, a variety of Hg^{2+} sensors based on small organic molecules (Ko et al., 2006), proteins (Hollenstein et al., 2008; Li et al., 2008; Liu and Lu, 2007) and genetically engineered bacteria (Ivask et al., 2001; Mertens et al., 2011) have been developed. One of the advances in Hg^{2+} detection is the discovery of thymine- Hg^{2+} -thymine (T- Hg^{2+} -T) coordination chemistry, whose stability is even higher than that of T-A Watson-Crick pair (Clever et al., 2007; Ono and Togashi, 2004; Saidura et al., 2017; Sugiyama et al., 2005; Tanaka et al., 2007; Xu et al., 2018). In addition, the T- Hg^{2+} -T interaction is highly specific. Based on the Hg^{2+} mediated T-T DNA base pairing, a variety of techniques for monitoring Hg^{2+} have been developed, including colorimetric method (Chen et al., 2014, 2015; Wei et al., 2014), fluorometric method (Duan et al., 2018; Guo et al., 2011; D. Liu et al., 2011; X. Liu et al., 2011; Wang et al., 2016; Yang et al., 2018; Jiang et al., 2014; Zhang et al., 2015) and electrochemical method (Cai et al., 2016; Miao et al., 2009; Park et al., 2012; Wu et al., 2016, 2018; Yuan et al., 2011; Zeng et al., 2017). However, the fluorometric method still needs a complicated and expensive instrumentation, though it has the high sensitivity. Electrochemical biosensor needs the immobilization of the probe on the electrode surface resulting in a complicated and time-consuming sample treatment process. Personal glucose meter based electrochemical biosensor is compact and rapid, however it requires invertase enzyme to convert sucrose into glucose, therefore the storage of the biosensor needs special care to keep the enzyme activity. Unfortunately, not only the classical Hg^{2+} detection methods, but also these approaches based on T- Hg^{2+} -T tactics do not suit for on-site Hg^{2+} detection due to their required huge and expensive instrumentation or complicated and time-consuming operations. In order to develop on-site Hg^{2+} detection methods, the gold nanoparticle based colorimetric assay is proposed (Lin et al., 2011; D. Liu et al., 2011; X. Liu et al., 2011), which can operate at room temperature using naked eyes, demonstrating the property of simplicity and rapidity, but their sensitivity is often poor. Since mobile sensing and imaging devices can realize precise detections especially for on-site applications due to their cost-effective and compact configurations (Coskun et al., 2013; Lee et al., 2014; Lin et al., 2017; Lu et al., 2017; Ludwig et al., 2014; Meng et al., 2017; Vashist et al., 2015; Wei et al., 2013; Zhu et al., 2013), combining with the smartphone based detection and analysis, the limit of detection (LoD) of the gold nanoparticle based colorimetric assay increased to 3.5 parts-per-billion (ppb) (Wei et al., 2014), however it is still above the upper limit of Hg^{2+} as 2 ppb (~ 10 nM) mandated by United States Environmental Protection Agency and 1 ppb (~ 5 nM) mandated by National Health Commission of the People's Republic of China. Therefore, there is still a strong desire to develop a miniaturized, sensitive, convenient and rapid system for on-site detection of Hg^{2+} in the environment or food.

Herein, we describe a smart Hg^{2+} detection method combining the fluorescence biosensor, the smartphone fluorescence microscope and the smartphone application. The fluorescence biosensor can capture the target and provide the fluorescence signal, and the smartphone fluorescence microscope as well as the smartphone application can localize and detect the fluorescence signal, thus providing quantitative Hg^{2+} detection. The fluorescence biosensor takes advantages of the selective T- Hg^{2+} -T interaction and the magnetic bead (MB) separation/collection process. Recently, the employment of MBs enables quick sorting of targets in high yield and purity, becoming essential tools for high-throughput and low-cost isolation of biomolecules in bio-sensing (Bi et al., 2015a, 2015b; Bi et al., 2016a, 2016b; Yue et al., 2017). Compared to other separation techniques, such as centrifugation, chromatographic separation and membrane separation, magnetic separation has the distinct advantages of fast and simple handling processes, high efficiency, and low cost. As shown in Fig. 1, the capture oligonucleotide strands containing Ts are immobilized on the streptavidin-coated Fe_3O_4 magnetic beads through biotin-streptavidin linkage, and the signal

oligonucleotide strands containing Ts are labeled with the carboxyl-coated polystyrene fluorescent microspheres (PFMs). MBs are used to separate the products for Hg^{2+} detection, and then the fluorescence signals are collected with the smartphone fluorescence microscope which is composed of excitation illumination, micro-objective and image recorder, and assembled with 3-D printing model. The miniaturized and cost-effective smartphone fluorescence microscope has the size of 170 mm (length) \times 113 mm (width) \times 168 mm (height), which is much smaller than commercial fluorescence microscopes; besides, it has the high resolution of 2.2 μm and the signal to noise ratio of 22 dB, proving it can collect the fluorescence signals in high precision and sensitivity. Moreover, a self-programmed smartphone application is adopted for fluorescence signal analysis to support the quantitative Hg^{2+} measurements. The detection operations are simple and rapid only with miniaturized and cost-effective devices, and the biosensor can be easily preserved. According to the practical measurements, a highly specific detection of Hg^{2+} with a linear relation between 1 nM and 1 μM , and a LoD of 1 nM can be obtained with the smart Hg^{2+} detection method. Additionally, we also adopt this method in Hg^{2+} contamination detection on the tap water collected from China. Considering the smart Hg^{2+} detection approach can realize sensitive and selective quantitative Hg^{2+} detection with simple operations and cost-effective system, it is believed the proposed method owns great potentials in Hg^{2+} detection for routine uses at home or in the field for food safety detection or water quality monitoring.

2. Materials and methods

2.1. Reagents

Tris (hydroxymethyl) aminomethane-hydrochloric acid (Tris-HCl) and Tween-20 purchased from Sigma-Aldrich (US), nitric acid (HNO_3), potassium chloride (KCl), potassium dihydrogen phosphate (KH_2PO_4), sodium chloride (NaCl), sodium bicarbonate (NaHCO_3), disodium hydrogen phosphate (Na_2HPO_4) and ethylenediaminetetraacetic acid (EDTA) purchased from Sinopharm (China) were of analytical grade and used without further purification. N-Hydroxysuccinimide (NHS) and N-(3-(dimethylamino)propyl)-N'-ethylcarbodiimide hydrochloride (EDC) were purchased from Sigma-Aldrich (US). Streptavidin-coated Fe_3O_4 magnetic beads were purchased from Suzhou Beaver Biomedical Engineering Co., Ltd. (China). Carboxyl-coated polystyrene fluorescent microspheres were purchased from Tianjin Baseline Chromtech Research Center Co. Ltd. (China). The glass slide for sample chamber was purchased from Thermo Fisher (US). The standard solutions of Hg^{2+} , Pb^{2+} , Mg^{2+} , Fe^{2+} , Fe^{3+} , Ca^{2+} , Zn^{2+} , K^+ , Ni^{2+} , Cd^{2+} and Co^{2+} were purchased from Beijing Spectrum Analysis Technology Co., Ltd. (China). Ultrapure water obtained from a Millipore water purification system (Milli-Q, Millipore, 18.2 MU resistivity) was used in experiments. All the oligonucleotides were synthesized by Shanghai Sangon Biotechnology Co., Ltd. (China). The capture probes and the signal probes were labeled with biotin and NH_2 at their 5'-ends, respectively. The sequence of the capture probe is 5'-Biotin-AAAAAAAAAACATGT TAGTCGTTGCT-3', and that of the signal probe is 5'- NH_2 -AGCTTCGT CTATCTTG-3'.

2.2. Influence of the Hg^{2+} on the fluorescence signals

First, 100 μL carboxyl-coated PFM ($D = \sim 0.7 \mu\text{m}$) solution (10 mg/mL) was centrifuged at 12,000 rpm for 5 min and washed with 400 μL Buffer I (pH = 7.2, NaCl 137 mM, KCl 2.7 mM, Na_2HPO_4 10 mM, KH_2PO_4 2 mM) for three times. The precipitate of the PFMs was then dissolved in 2 mL aqueous solutions (3% HNO_3) of Hg^{2+} with the concentrations of 10 nM, 50 nM, 100 nM, 1 μM , 2 μM , 10 μM and 100 μM , respectively. Hg^{2+} concentrations were quantitatively measured via the atomic fluorescence spectrometer (Persee, Beijing, China). Finally, at 0, 4, 8, 12, 16, 20, 24 and 28 min, 200 μL of these mixed

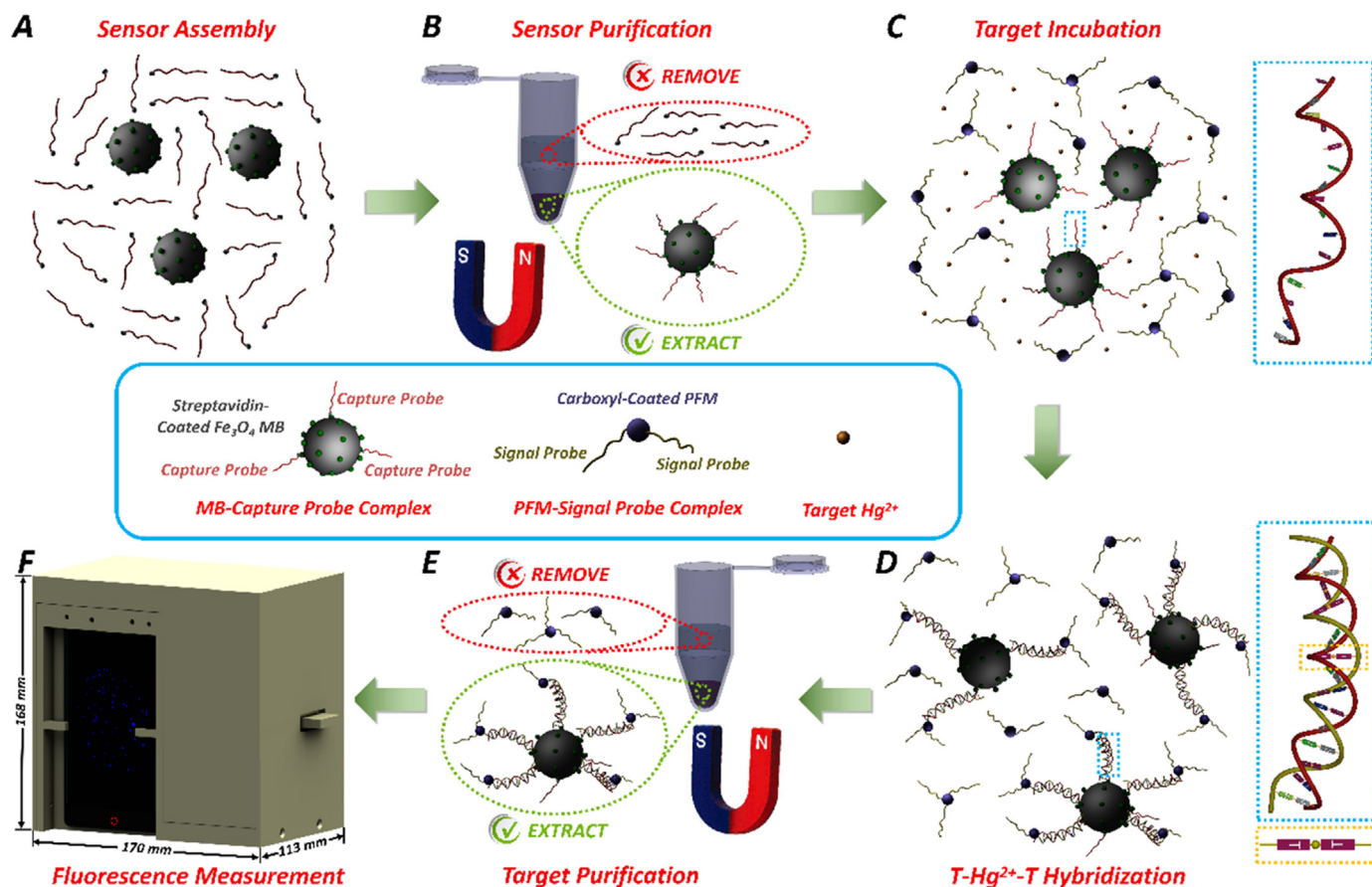


Fig. 1. Detection principle of the smart Hg^{2+} detection method. (A) Sensor assembly. (B) Sensor purification. (C) Target incubation. (D) T- Hg^{2+} -T hybridization. (E) Target purification. (F) Fluorescence measurements. The size of the proposed smartphone fluorescence microscope is marked in (F).

solutions were transferred to 96-well plates, and their fluorescence signals were measured with the multi-label counter (Tecan, Switzerland) with the excitation wavelength of 405 nm and the emission wavelength of 450 nm to quantitatively analyze the fluorescence signals influenced by Hg^{2+} concentrations.

2.3. Conjugation between the capture probes and the streptavidin-coated Fe_3O_4 MBs

First, 50 μL streptavidin-coated Fe_3O_4 MBs ($D = \sim 2 \mu\text{m}$, 10 mg/mL) were washed three times by 450 μL Buffer II (pH = 7.2, 10 mM Tris-HCl, 1 mM EDTA, 1 M NaCl, 0.01–0.1% Tween-20) through a magnetic separation device. Next, the precipitate of the MBs was incubated with 500 μL Buffer II containing 2 μM biotinylated capture probes with gently shaking for 30 min at room temperature as shown in Fig. 1(A), and the MB-capture probe complexes were finally separated using a magnetic separation device as shown in Fig. 1(B). The connection between the streptavidin-coated Fe_3O_4 MBs and the biotinylated capture probes was confirmed by dynamic light scattering (DLS, Malvern, UK) and zeta potentials (Malvern, UK).

2.4. Conjugation between the signal probes and the carboxyl-coated PFMs

100 μL carboxyl-coated PFM solution (10 mg/mL) was centrifuged at 12,000 rpm for 5 min and washed with Buffer III (pH = 6.8, NaCl 137 mM, KCl 2.7 mM, Na_2HPO_4 10 mM, KH_2PO_4 2 mM) for three times. The precipitate of the PFMs was then activated in 500 μL Buffer III with 30 mM EDC and NHS with gently shaking for 30 min at room temperature. The activated PFMs were centrifuged at 12,000 rpm for 5 min and washed with 500 μL Buffer I for two times. The precipitate of the

activated PFMs was suspended in 400 μL Buffer I and linked with 100 μL amine-modified signal probes (500 nM) with gently shaking for 3 h at 37 $^\circ\text{C}$ to generate the fluorescently labeled signal probes, which were centrifuged at 12,000 rpm for 5 min and washed with Buffer I for three times afterwards. Finally, the precipitate of the fluorescently labeled signal probes was suspended with Buffer I and the connection between the PFMs and the signal probes were confirmed by DLS (Malvern, UK) and zeta potentials (Zetasizer, Malvern, UK).

2.5. Hg^{2+} detection

To measure the Hg^{2+} concentrations with the smart Hg^{2+} detection method, 50 μL solution containing Hg^{2+} was first mixed with 10 μL prepared MB-capture probe complexes and 20 μL prepared PFM-signal probe complexes for incubation at room temperature for 20 min as shown in Fig. 1(C) and (D). The incubated products were washed three times with 500 μL Buffer I through a magnetic separation device as shown in Fig. 1(E). The precipitate was suspended with 20 μL Buffer I and applied to the glass sample chamber for fluorescence signals collection at $\sim 450 \text{ nm}$ with the smartphone fluorescence microscope as shown in Fig. 1(F). Moreover, the fluorescence emission spectra of the final complexes with different concentrations of Hg^{2+} were also measured with the multi-label counter (Tecan, Switzerland) to ensure that there are no significant shifts of the emission spectra induced by the Hg^{2+} .

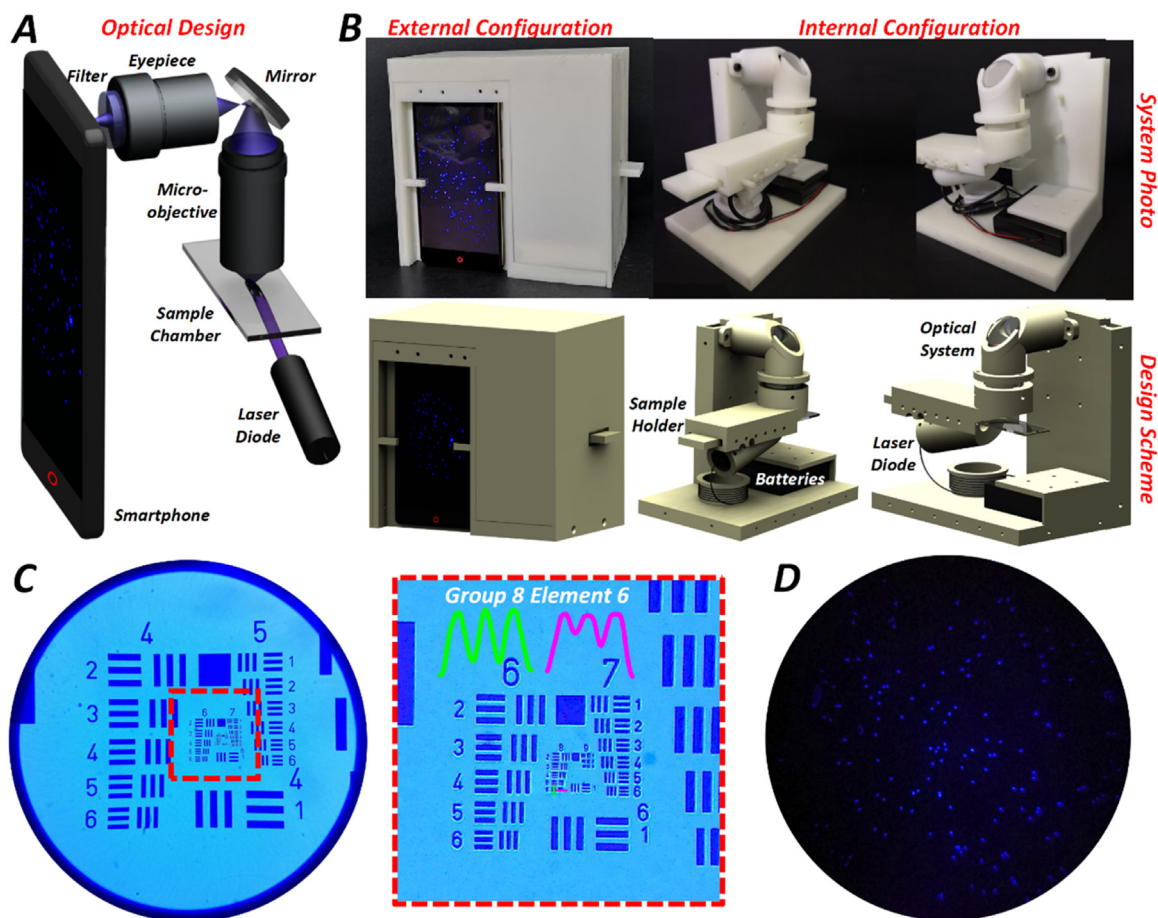


Fig. 2. Smartphone fluorescence microscope. (A) Optical design of the smartphone fluorescence microscope. (B) System photo and design sketch of the smartphone fluorescence microscope. (C) Resolution and FoV estimation using the 1951 USAF resolution test chart. (D) Signal to noise ratio estimation using the fluorescent bead imaging.

3. Results

3.1. Smartphone fluorescence microscope

To collect the fluorescence signals to quantitatively evaluate the Hg^{2+} concentration, the optical system, which is a smartphone fluorescence microscope, was designed as shown in Fig. 2(A). A laser diode (Haoran Optics, China) with the wavelength of 405 nm and the power of 100 mW supplied by batteries acted as the excitation source, and the excitation light was a tilted laser illuminated to the sample chamber to excite the fluorescence signals in order to improve the signal to noise ratio by avoiding the collection of the excitation light by the micro-objective. A $20\times$ micro-objective (Daheng Optics, China) was used for sample magnification, and an eyepiece (Edmund Optics, US) was adopted for connecting the smartphone camera and the micro-objective. Before the smartphone camera, an emission filter (Thorlabs, US) with the central wavelength of 469 nm and the band width of 35 nm was set in order to remove the scattered excitation light. Besides, a reflective mirror (Daheng Optics, China) was inserted into the optical system for optical system bending in order to reduce the system size. The fluorescence image was then captured by a smartphone (Z17 mini, Nubia, China) with the fixed exposure time of 0.3 s. Since the power of the excitation laser is fixed, the exposure time is determined according to the collected fluorescence signals when the Hg^{2+} concentration is $1\ \mu\text{M}$. In this condition, by adjusting the exposure time of the smartphone, the collected fluorescence signals should lower than but close to 255 in order pursue high signal to noise ratio but to avoid the over-exposure as the captured fluorescence intensity is an 8-bit image.

Next to integrate these optical elements, a 3-D printing model was fabricated to assemble the miniaturized smartphone fluorescence microscopes as shown in Fig. 2(B) with the size of 170 mm (length) \times 113 mm (width) \times 168 mm (height), which is much more compact than the commercial fluorescence microscopes. Moreover, the laser diode is supplied by batteries in the smartphone fluorescence microscope, thus no external power supply is required. Fig. 2(B) also reveals the inner configuration of the optical system, which was covered with a shell in measurements in order to avoid the environmental light. The tilting illuminated laser diode was set on the sample holder module, and its tilting illumination angle could be slightly adjusted by the positioning screw. The glass sample chamber carried by the sample holder could be adjusted in both X and Y axes for field of view (FoV) scanning by moving the sample chamber connector, and it also could be adjusted in Z axis for focus adjustment by the whole sample holder translation. The optical elements including the micro-objective, the eyepiece, the emission filter and the reflective mirror were integrated in the optical module, and connecting with the smartphone, the fluorescence signals could be collected. It is worth noting that the tilting illumination angle and the focal plane can be well adjusted before Hg^{2+} detection, and after covered with the shell, the sample chamber could still be scanned in both X and Y directions to enlarge the FoV by adjusting the sample chamber connector.

Before the smartphone fluorescence microscope was used for Hg^{2+} detection, its imaging quality was first tested using a 1951 USAF resolution test chart (Edmund Optics, USA). In this testing, the light source was changed into a blue LED with the central wavelength of 451 nm and the band width of 10 nm (Daheng Optics, China). Fig. 2(C)

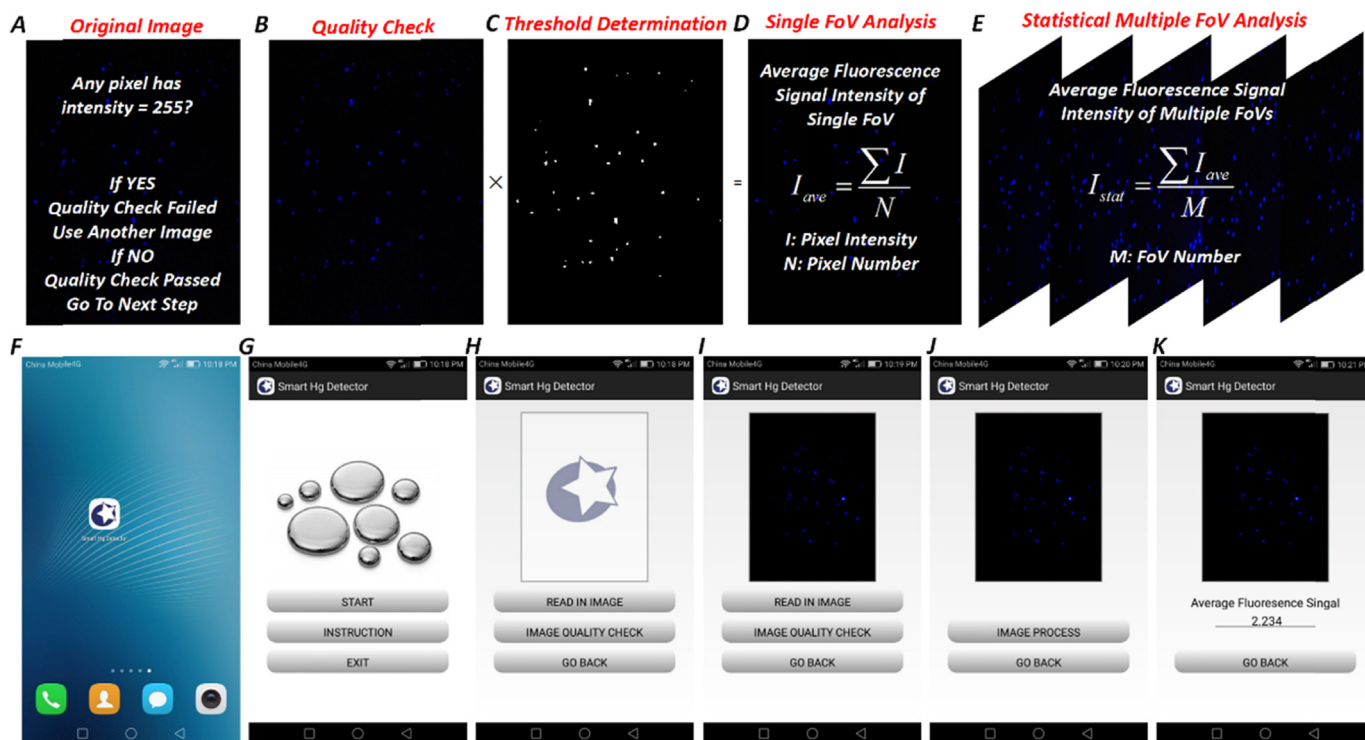


Fig. 3. Smartphone application. (A)–(E) Flow-chart of the data analysis algorithm. (A) Captured fluorescence image. (B) Fluorescence image after quality check. (C) Threshold mask for thresholding segmentation. (D) Single FoV analysis. (E) Statistical multiple FoV analysis. (F)–(K) Smartphone application. (F) Application icon in the smartphone desktop. (G) Initial interface. (H) Fluorescence image read-in interface. (I) Fluorescence image quality check interface. (J) Image process interface. (K) Average fluorescence signal intensity within the FoV computation interface.

shows the recorded image, indicating that the system could reach the resolution of $2.2\ \mu\text{m}$ according to its resolved line pair of Group 8 Element 6. Moreover, the FoV of the smartphone fluorescence microscope reached $1.5\ \text{mm}^2$ according to the USAF resolution test chart imaging. Next, the fluorescent microspheres were also used for imaging quality testing, according to the captured image shown in Fig. 2(D), it has rather high signal to noise ratio of $\sim 22\ \text{dB}$ combining with the tilted illumination excitation light and the emission filter, proving the miniaturized smartphone fluorescence microscope can record high-quality fluorescence images with high resolution and signal to noise ratio.

3.2. Smartphone application

After capturing the fluorescence image, the Hg^{2+} concentration can be evaluated via the average fluorescence signal intensity. Fig. 3(A) to (E) shows the data analysis algorithm for statistical average fluorescence signal intensity computation. Specifically, Fig. 3(A) shows the captured fluorescence image with the fixed exposure time of 0.3 s, and it first requires quality check: if there is no pixel with the value of 255, the fluorescence image could be further used for fluorescence signal analysis, otherwise, this fluorescence image should be abandoned. According to the fluorescence signal intensity after quality check in Fig. 3(B), a threshold mask is generated according to the classical thresholding segmentation method (Gonzalez and Woods, 2017) as shown in Fig. 3(C), which is a binary pattern composed of 0 and 1. Fig. 3(D) is the multiplication of Fig. 3(B) and (C), and the multiplication result keeps the fluorescence signals but obviously reduces the background. For this single FoV, the average fluorescence signal intensity is computed as Eq. (1), in which I_{ave} is the average fluorescence signal intensity in a single FoV, I is the pixel intensity within the FoV and N is the pixel number of the FoV.

$$I_{ave} = \frac{\sum I}{N} \quad (1)$$

In order to further reduce the detection error, especially for low Hg^{2+} concentration evaluation, more sampling is preferred, therefore multiple FoVs in a sample chamber were used for average fluorescence signal intensity measurements. The statistical average fluorescence signal intensity for final Hg^{2+} concentration measurements is calculated according to Eq. (2), in which I_{stat} is the statistical average fluorescence signal intensity of multiple FoVs, and M is the number of FoVs used in statistical analysis.

$$I_{stat} = \frac{\sum I_{ave}}{M} \quad (2)$$

Moreover, a smartphone application was designed as shown in Fig. 3(F) to (K) to support the quantitative Hg^{2+} measurements based on the data analysis algorithm shown in Fig. 3(A) to (E). In this application, first, after opening the application as shown in Fig. 3(F) and (G), it could load the recorded 8-bit fluorescence image as shown in Fig. 3(H). Then, the quality of the fluorescence image was checked in order to avoid the over-exposure as shown in Fig. 3(I). Finally, the average fluorescence signal intensity was calculated to quantitatively estimate the Hg^{2+} concentration. Fig. 3(J) and (K) show the average fluorescence signal intensity of a single FoV, and the statistical average fluorescence signal intensity can be computed from multiple FoVs in order to evaluate the Hg^{2+} concentration in high accuracy. It is known that when enough sampling is obtained, accurate Hg^{2+} concentration can be estimated even from statistical average fluorescence signal intensity obtained from only a few FoVs, since the sampling tactic for Hg^{2+} concentration estimation is equivalent to that based on all the fluorescence collections. But our used method not only reduces the time consumed due to the less FoV detections, but also avoids the error caused by overlapping and missing in FoV stitching for all the fluorescence collections, since FoVs are circular areas.

3.3. Hg^{2+} detection using the smart Hg^{2+} detection approach

To detect the Hg^{2+} in the solution, the MB-capture probe complexes and the PFM-signal probe complexes were incubated with Hg^{2+} aqueous solution as described in the Materials and Methods section. The prepared MB-capture probe complexes and the prepared PFM-signal probe complexes are easy to store and can be preserved for more than 6 months. The magnetic separated products were suspended with Buffer I and applied to the glass sample chamber for fluorescence signals collection at ~ 450 nm with the smart Hg^{2+} detection method. With the fixed exposure time of 0.3 s of the smartphone fluorescence microscope, fluorescence images in various FoVs were captured of a single sample by scanning the sample chamber to increase sampling. Using the application, the captured fluorescence images were analyzed to compute the average fluorescence signal intensity within the FoV to support the quantitative Hg^{2+} concentration measurements. During the fluorescence image processing, for a single sample, the fluorescence image in different FoVs should be analyzed in order to obtain the stable results, and during this procedure, some over-exposure fluorescence images should be excluded. However, if most of the captured fluorescence images are over-exposure, one reason is that the Hg^{2+} concentration is higher than $1 \mu\text{M}$ which is the upper bound of the detection range, and the sample should be diluted for Hg^{2+} concentration measurements; another reason is that the fluorescence biosensor accumulates, and in this case, the fluorescence biosensor should be re-produced.

Including the optimized sample incubation (shown in Fig. 4(E) in details), target extraction, signal collection and analysis, the whole procedures for Hg^{2+} concentration measurements can be finished within 30 min, indicating that Hg^{2+} can be rapidly detected; besides, noting that the magnetic separation device and the smartphone fluorescence microscope required for Hg^{2+} detection are all miniaturized and cost-effective, and the smartphone fluorescence microscope has self-supplied internal power, thus no external power supply is required, therefore, it is believed the proposed smart Hg^{2+} detection method can be implemented for the rapid on-site detection.

3.4. Certification and optimization of the designed fluorescence biosensor

Before analyzing the performance of the smart Hg^{2+} detection approach, the designed fluorescence biosensor was certificated and optimized. First, the connections between the streptavidin-coated Fe_3O_4 MBs and the capture probes as well as the connections between the carboxyl-coated PFMs and the signal probes were characterized by DLS. According to Fig. 4(A), the average hydrodynamic diameter of the streptavidin-coated Fe_3O_4 MBs is 1916 nm with the full width at half maximum (FWHM) of 1032 nm, while the average hydrodynamic diameter of the MB-capture probe complexes is 2023 nm with the FWHM of 1139 nm. The obvious increase in the hydrodynamic diameter indicates that the capture probes were successfully conjugated to the MBs. Similarly, Fig. 4(A) also shows that the average hydrodynamic diameters of the carboxyl-coated PFMs and the PFM-signal probe complexes are 749 nm and 828 nm with the FWHMs of 433 nm and 373 nm, respectively, indicating the successful conjugation of the carboxyl-coated PFMs with the signal probes. We further measured the zeta potentials of the MBs, the MB-capture probe complexes, the PFMs and the PFM-signal probe complexes, respectively. The results are listed in Fig. 4(B) showing that there were significant changes in the zeta potential upon connection of capture probes with the MBs and signal probes with PFMs. Together these data demonstrated the successful connection between the capture probes with the MBs and the signal probes with PFMs.

Then, the influence of Hg^{2+} on the fluorescence signals was also studied. The PFMs were dissolved in aqueous solutions (3% HNO_3) with Hg^{2+} concentrations of 10 nM, 50 nM, 100 nM, $1 \mu\text{M}$, $2 \mu\text{M}$, $10 \mu\text{M}$ and $100 \mu\text{M}$, respectively, and their corresponding fluorescence signals at 450 nm were measured at 0, 4, 8, 12, 16, 20, 24 and 28 min by the

multi-label counter (Tecan, Switzerland). According to the measured fluorescence signals listed in Fig. 4(C), the Hg^{2+} almost has no impact on the fluorescence signals even with the rather high Hg^{2+} concentration of $1 \mu\text{M}$. Considering that the measuring range of the proposed biosensor was up to $1 \mu\text{M}$ in this work, the influence of Hg^{2+} on the fluorescence signals could be ignored during fluorescence signal detections.

Next, the feasibility of the designed fluorescence biosensor for Hg^{2+} detection was certificated using the smartphone fluorescence microscope as shown in Fig. 4(D). For each sample, 5 glass sample chambers were used, and for each glass sample chamber, 5 FoVs were captured, therefore, totally 25 FoVs were measured. When there was no Hg^{2+} , the statistical average fluorescence signal was rather low as around 0.1 which is treated as the background level. When 200 nM Hg^{2+} was introduced, but the capture probes or the signal probes were missing, the statistical average fluorescence signals were both low and close to the background level proved by the *t*-test. While when the biosensor was complete, the statistical average fluorescence signal reached 0.56 ± 0.06 ; and according to the *t*-test, the *p* value between the fluorescence signals without and with Hg^{2+} was lower than 0.05, indicating that only the complete biosensor including MB-capture probe complexes and PFM-signal probe complexes could realize the Hg^{2+} detection. When the Hg^{2+} concentration increased to 600 nM, obvious higher statistical average fluorescence signal as 1.71 ± 0.17 was obtained, proving the designed fluorescence biosensor could be potentially adopted in quantitative Hg^{2+} concentration measurements.

Moreover, to accelerate the detecting process as well as to pursue higher signal to noise ratio, the incubation time of Hg^{2+} solution and the biosensor system was also optimized as shown in Fig. 4(E) with the Hg^{2+} concentrations of 10 nM, 50 nM, 100 nM and 400 nM from low to high concentrations. Similarly, for each condition, 5 glass sample chambers were used, and for each glass sample chamber, 5 FoVs were captured. The statistical average fluorescence signals increased till the incubation time reached 20 min; however, the statistical average fluorescence signals kept stable after 20 min, since the *p* values between the fluorescence signals at 20 min and those at 25 min in different Hg^{2+} concentrations were all higher than 0.05. The results proved that the incubation time should be set as 20 min in order to acquire high fluorescence signals and to reduce the processing time.

Finally, measured by multi-label counter (Tecan, Switzerland), the fluorescence emission spectra of the final complexes with different concentrations of Hg^{2+} is shown Fig. 4(F). Though the spectra blue-shift with higher Hg^{2+} concentrations, the shifts are rather small, and according to the adopted emission filter, the fluorescence signals around the emission peak at ~ 450 nm can still be collected for precise Hg^{2+} detections.

3.5. Performance of the smart Hg^{2+} detection approach

First, the relation between the Hg^{2+} concentration and the fluorescence signal was quantitatively calibrated. Hg^{2+} aqueous solutions with different concentrations from 0.1 nM to $1 \mu\text{M}$ were used as samples, respectively, and the statistical average fluorescence signal intensities within the FoV corresponding to different Hg^{2+} concentrations were illustrated in Fig. 5(A). For each sample, 5 glass sample chambers were used, and for each glass sample chamber, 5 FoVs were captured, therefore, the statistical average fluorescence signal was retrieved from totally 25 FoVs were measured. In this research, the LoD was defined as the fluorescence signal of background plus 3 times standard deviation, based on which the LoD of the Hg^{2+} concentration was obtained as 1 nM, since the statistical average fluorescence signal corresponding to the LoD (~ 0.15) was just higher than the fluorescence signal of background plus 3 times standard deviation. Additionally, the LoD was also proved by *t*-test, the *p* value between the fluorescence signals of the Hg^{2+} concentrations of 1 nM and those without Hg^{2+} was lower than 0.05; however, the *p* value between the fluorescence signals of the

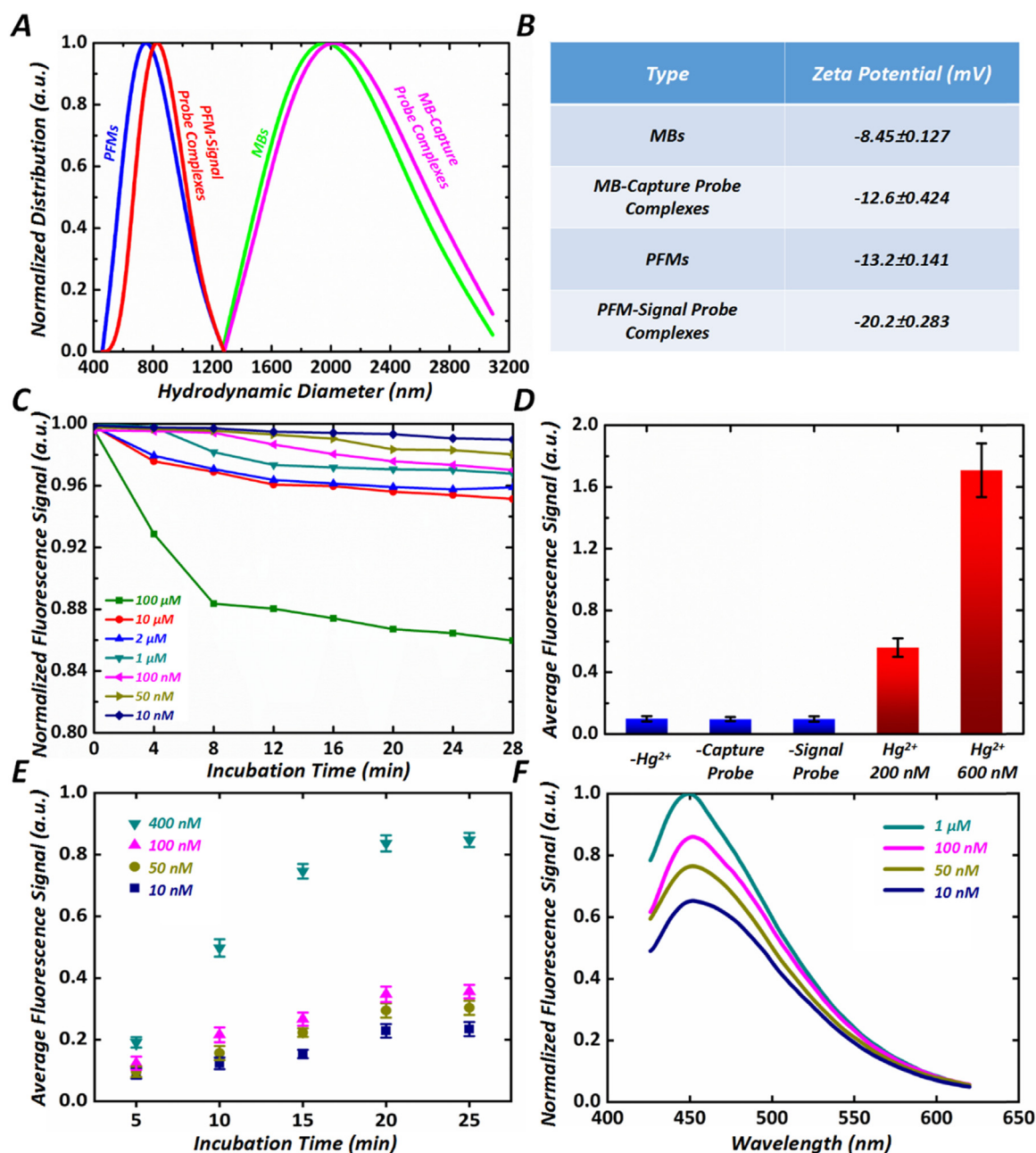


Fig. 4. Certification and optimization of the designed fluorescence biosensor. (A) Hydrodynamic diameter distributions of MBs, MB-capture probe complexes, PFMs and PFM-signal probe complexes measured by DLS. (B) Zeta potentials of MBs, MB-capture probe complexes, PFMs and PFM-signal probe complexes. (C) Fluorescence signals with different Hg^{2+} concentrations. (D) Fluorescence signals in different conditions without capture probes or signal probes and with the complete biosensor system. (E) Fluorescence signals at different incubation time of the Hg^{2+} solution with the biosensor system. (F) The fluorescence emission spectra with different Hg^{2+} concentrations.

Hg^{2+} concentrations of 0.1 nM and those without Hg^{2+} was higher than 0.05. It is worth noting that the LoD is much lower than the China and US standards for tap water. Besides, comparisons of the sensitivity of our smart Hg^{2+} detection method with other published bio-sensing approaches based on T- Hg^{2+} -T coordination chemistry show that the LoD of the smart Hg^{2+} detection method is as good as or better than many recently published bio-sensing approaches as shown in Table 1. Moreover, the detected fluorescence signals increased significantly with higher Hg^{2+} concentration, and with the linear fitting, it is found that when the Hg^{2+} concentration range is between 1 nM and 1 μM , the average fluorescence signal intensity within the FoV increased almost linearly with higher Hg^{2+} concentrations as shown in the inset of Fig. 5(A), therefore, it is proved that the proposed smart Hg^{2+} detection

method can be adopted for quantitative Hg^{2+} concentration measurements according to a high regression coefficient of 0.9798.

Then, according to the calibrated linear relation between the Hg^{2+} concentration and the average fluorescence signal intensity within the FoV, the detecting accuracy on the Hg^{2+} concentration of the smart Hg^{2+} detection method was evaluated. Hg^{2+} aqueous solutions with different concentrations as 140 nM, 100 nM, 40 nM and 10 nM were prepared as samples. Using both the smart Hg^{2+} detection method and the atomic fluorescence spectrometer (Beijing Haiguang Instruments Co., Ltd., China), the detection results were compared in Fig. 5(B). Here, the Hg^{2+} concentrations were computed from 5 measurements using the atomic fluorescence spectrometer, and calculated from 25 FoVs using the proposed smart Hg^{2+} detection method. For all the

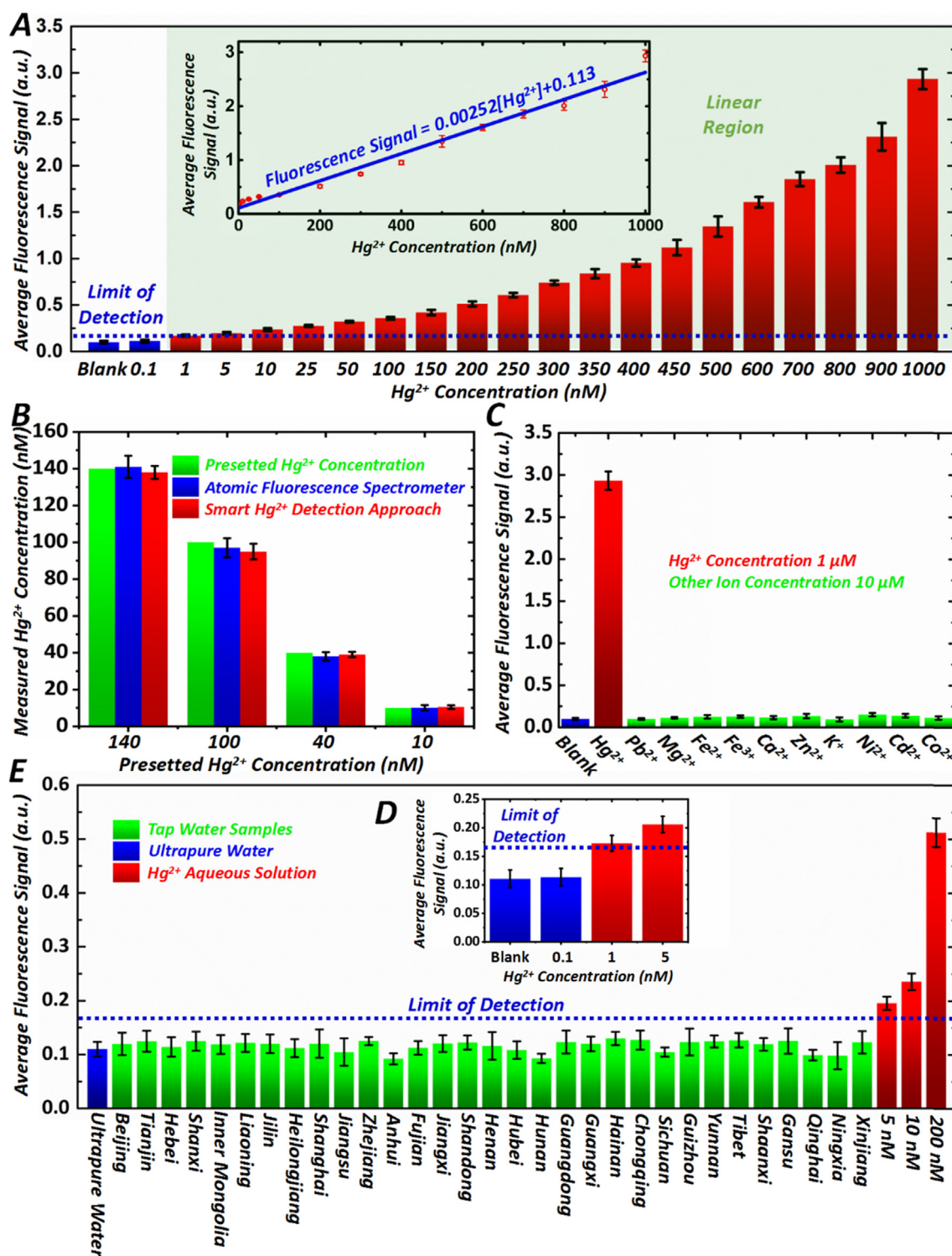


Fig. 5. Performance of the smart Hg^{2+} detection method. (A) Quantitative calibration between the Hg^{2+} concentration and the fluorescence signal. (B) Accuracy testing on the Hg^{2+} concentration of the smart Hg^{2+} detection method. (C) Specificity testing by measuring fluorescence signals of different metal ions. (D) Quantitative LoD calibration of the tap water samples. (E) Measured results of tap water samples.

samples with different Hg^{2+} concentrations, the measured concentrations obtained by the proposed smart Hg^{2+} detection method were rather close to the presetted concentrations as well as those measured by classical atomic fluorescence spectrometer, proving that the proposed smart Hg^{2+} detection method can provide quantitative Hg^{2+} concentration measurements in high accuracy.

In addition, the specificity of the smart Hg^{2+} detection method was

evaluated. Hg^{2+} aqueous solutions with the concentration of 1 μM and Pb^{2+} , Mg^{2+} , Fe^{2+} , Fe^{3+} , Ca^{2+} , Zn^{2+} , K^+ , Ni^{2+} , Cd^{2+} , Co^{2+} aqueous solutions with rather high concentration of 10 μM were measured using the proposed smart Hg^{2+} detection method, and the statistical average fluorescence signals obtained from 25 FoVs in each case were listed in Fig. 5(C). According to the statistical analysis, the p value between the fluorescence signals of the Hg^{2+} concentrations of 1 μM and those of

Table 1
Comparisons on the sensors for Hg²⁺ detections.

Method	Reagent	Linear range(nM)	Detection limit(nM)	Sample type	Ref.
Fluorescence	Microspheres	1–1000	1	Tap water	This work
Fluorescence	QDs/AuNPs	10–400	6.6	Tap water	Jiang et al. (2014)
Fluorescence	aptamer	5–150	0.42	River and Tap water	Zhang et al. (2015)
Colorimetric method	AuNPs	10–1000	17.3	Rivers, Lakes, and Beaches	Wei et al. (2014)
Colorimetric method	AuNPs	25–750	50	Pond and River water	Chen et al. (2014)
Colorimetric method	AuNPs	10–2000	7.1	Lake water	Chen et al. (2015)
Electrochemistry	AuNPs	1–200	0.33	Lake water	Wu et al. (2016)

blank condition was lower than 0.05; however, the *p* values between the fluorescence signals of other metal ions and those of blank condition were all higher than 0.05. It shows that the high statistical average fluorescence signal could only be obtained when Hg²⁺ existed, while the statistical average fluorescence signals of all other metal ions tested were close to the background level. Through the proposed quantitative specificity evaluation, it is believed that the smart Hg²⁺ detection method can detect target Hg²⁺ with rather high selectivity.

According to the performance certification of the proposed smart Hg²⁺ detection method, Hg²⁺ concentration can be quantitatively measured in low LoD, high accuracy and excellent specificity. Especially the LoD is lower than the China and US standards, the smart Hg²⁺ detection method was next adopted for Hg²⁺ contamination detection in tap water.

3.6. Application of the smart Hg²⁺ detection approach

As an application, the proposed smart Hg²⁺ detection method was adopted for Hg²⁺ contamination detection in tap water collected from China. Moreover, ultrapure water and aqueous solutions with the Hg²⁺ concentrations of 5 nM, 10 nM and 200 nM were also detected as comparisons. Before tap water detection, the LoD of real sample was determined. The tap water in Nanjing was first measured by atomic fluorescence spectrometer (Beijing Haiguang Instruments Co., Ltd., China), and proved there was no Hg²⁺ in the tap water. Next, Hg²⁺ was introduced to the Hg²⁺ free tap water, and the statistical average fluorescence signals obtained from 25 FoVs corresponding to 0 nM, 0.1 nM, 1 nM and 5 nM Hg²⁺ are shown in Fig. 5(D). In real sample condition, the LoD of the Hg²⁺ concentration was also 1 nM, since the statistical average fluorescence signal corresponding to the LoD was higher than the fluorescence signal of background plus 3 times standard deviation as 0.165 in real sample. Additionally, the LoD of real sample was also proved by *t*-test, the *p* values between the fluorescence signals of the Hg²⁺ concentrations of 1 or 5 nM and those without Hg²⁺ were lower than 0.05; however, the *p* value between the fluorescence signals of the Hg²⁺ concentrations of 0.1 nM and those without Hg²⁺ was higher than 0.05. According to the measured results shown in Fig. 5(E), Hg²⁺ aqueous solution with the concentrations of 5 nM, 10 nM and 200 nM could be distinguished, since their average fluorescence signals were both above the detection threshold as 0.165. While the statistical average fluorescence signals of all the tap water samples were close to the background fluorescence signal level, which are all below the fluorescence signal detection threshold, proving that Hg²⁺ could not be detected in the tap water samples collected from China.

4. Conclusion

In this paper, we design a smart Hg²⁺ detection approach using the fluorescence biosensor relying on T-Hg²⁺-T coordination chemistry to selectively and sensitively capture the Hg²⁺ in aqueous solution, the smartphone fluorescence microscope for collecting fluorescence signals from fluorescently labeled targets and the smartphone application for quantitative Hg²⁺ concentration measurements by analyzing the collected fluorescence signals. Only relying on the miniaturized and

inexpensive magnetic separation, the targets can be extracted rapidly and simply using the designed fluorescence biosensor within 30 min. Moreover, the smartphone fluorescence microscope is miniaturized and cost-effective, which has rather high imaging resolution of 2.2 μm and signal to noise ratio of 22 dB, but only with the compact size of 170 mm × 113 mm × 168 mm and self-supplied internal power. Besides, the self-programmed smartphone application can automatically recognize and analyze the fluorescence signals in order to support the quantitative Hg²⁺ measurements. Using the smart Hg²⁺ detection method, a highly specific detection of Hg²⁺ with a linear relation between 1 nM and 1 μM is obtained with a rather low LoD of 1 nM which is below the upper limit of 2 ppb (~10 nM) mandated by United States Environmental Protection Agency and 1 ppb (~5 nM) mandated by National Health Commission of the People's Republic of China, and it is successfully adopted for Hg²⁺ contamination detection in the tap water samples. Improvements such as combining with microfluidics, multiple channels can be fabricated in a single detection chip, thus it is potential to realize high-throughput detections. Moreover, developing handheld smartphone fluorescence detector and internet based smartphone application can further extend future application of the proposed smart Hg²⁺ detection method. Nonetheless here combining with the fluorescence biosensor and the miniaturized smartphone fluorescence microscope, the proposed smart Hg²⁺ detection method can realize sensitive and selective Hg²⁺ detection with simple operations and cost-effective system. It is believed that the smart Hg²⁺ detection method owns great potentials in Hg²⁺ detection for routine uses at home and on-site in the field for water quality or food safety monitoring.

CRedit authorship contribution statement

Yanke Shan: Data curation, Formal analysis, Methodology, Validation, Writing - original draft, Writing - review & editing. **Bin Wang:** Data curation, Formal analysis, Methodology, Validation, Writing - original draft, Writing - review & editing. **Huachuan Huang:** Resources, Software. **Dan Jian:** Resources, Software. **Xuping Wu:** Formal analysis. **Liang Xue:** Formal analysis. **Shouyu Wang:** Conceptualization, Funding acquisition, Investigation, Supervision, Validation, Writing - original draft, Writing - review & editing. **Fei Liu:** Conceptualization, Funding acquisition, Investigation, Supervision, Validation, Writing - original draft, Writing - review & editing.

Acknowledgements

The work is supported by National Natural Science Foundation of China (31870154, 31522056, 61705092); National Key Research and Development Program (2015BAD12B01, 2018YFD0500100); Natural Science Foundation of Jiangsu Province of China (BK20170194); Shanghai Sailing Program (17YF1407000) and the Priority Academic Program Development of Jiangsu Higher Education Institutions (PAPD). Authors thanks Xiaolin Feng, Ying Jin, Ting Liu, Yidan Long, Jie Meng, Peng Qiu, Aihui Sun, Nan Sun, Qi Wei, Miao Yu, Mingyuan Zhang, Bangming Zong for providing tap water samples from different places of China.

Author contributions

F.L. and S.W. conceived the idea and supervised the project; Y.S. and B.W. built the optical system and did experiments, Y.S., B.W., X.W. and L.X. analyzed data; H.H. designed and fabricated the 3-D printed shell; D.J. developed the Android application; all the authors wrote and revised the manuscript.

Declaration of interests

Prof. Fei Liu and Prof. Shouyu Wang have financial interests in Sinmotec LLC, a company that commercializes single molecule sensing and imaging techniques.

References

- Ai, H., 2014. *Sensors* 14, 17829–17831.
- Ai, X., Wang, Y., Hou, X., Yang, L., Zheng, C., Wu, L., 2013. *Analyst* 138, 3494–3501.
- Baughman, T.A., 2006. *Environ. Health Perspect.* 114, 147–152.
- Bi, S., Jia, X., Ye, J., Dong, Y., 2015a. *Biosens. Bioelectron.* 71, 427–433.
- Bi, S., Ye, J., Dong, Y., Li, H., Cao, W., 2016a. *Chem. Commun.* 52, 402–405.
- Bi, S., Yue, S., Song, W., Zhang, S., 2016b. *Chem. Commun.* 52, 12841–12844.
- Bi, S., Zhang, Z., Dong, Y., Wang, Z., 2015b. *Biosens. Bioelectron.* 65, 139–144.
- Boening, D.W., 2000. *Chemosphere* 40, 1335–1351.
- Cai, L., Guo, Z., Zheng, X., 2016. *Microchim. Acta* 183, 2345–2351.
- Chandra, P., 2016. *Nanobiosensors for Personalized and Onsite Biomedical Diagnosis*, 1st ed. IET Book, London.
- Chen, G., Chen, W., Yen, Y., Wang, C., Chang, H., Chen, C., 2014. *Anal. Chem.* 86, 6843–6849.
- Chen, H., Zhang, X., Sun, H., Sun, X., Shi, Y., Xu, S., Tang, Y., 2015. *Analyst* 140, 7170–7174.
- Clever, G.H., Kaul, C., Carell, T., 2007. *Angew. Chem. Int. Ed.* 46, 6226–6236.
- Coskun, A.F., Wong, J., Khodadadi, D., Nagi, R., Teya, A., Ozcan, A., 2013. *Lab. Chip* 13, 636–640.
- Duan, Z., Zhang, X., Ye, T., Zhang, X., Dong, S., Liu, J., Xiao, X., Jiang, C., 2018. *ACS Appl. Mater. Interfaces* 10, 25737–25743.
- Gonzalez, R.C., Woods, R.E., 2017. *Digital Image Processing*, 4th ed. Pearson, London.
- Guo, L., Yin, N., Chen, G., 2011. *J. Phys. Chem. C* 115, 4837–4842.
- Han, F.X., Patterson, W.D., Xia, Y., Sridhar, B.B.M., Su, Y., 2006. *Water Air Soil Pollut.* 170, 161–171.
- Hollenstein, M., Hipolito, C., Lam, C., Dietrich, D., Perrin, D.M., 2008. *Angew. Chem. Int. Ed.* 47, 4346–4350.
- Hoyle, I., Handy, R.D., 2005. *Aquat. Toxicol.* 72, 147–159.
- Ivask, A., Hakkila, K., Virta, M., 2001. *Anal. Chem.* 73, 5168–5171.
- Jiang, Y., Tian, J., Hu, K., Zhao, Y., Zhao, S., 2014. *Microchim. Acta* 181, 1423–1430.
- Ko, S.K., Yang, Y.K., Tae, J., Shin, I., 2006. *J. Am. Chem. Soc.* 128, 14150–14155.
- Kunkel, R., Manahan, S.E., 1973. *Anal. Chem.* 45, 1465–1468.
- Lee, S., Oncescu, V., Mancuso, M., Mehta, S., Erickson, D., 2014. *Lab. Chip* 14, 1437–1442.
- Li, D., Wieckowska, A., Willner, I., 2008. *Angew. Chem. Int. Ed.* 47, 3927–3931.
- Li, Q., Zhou, X., Xing, D., 2010. *Biosens. Bioelectron.* 26, 859–862.
- Li, Y., Chen, C., Li, B., Sun, J., Wang, J., Gao, Y., Zhao, Y., Chai, Z., 2006. *J. Anal. At. Spectrom.* 21, 94–96.
- Lin, H.Y., Huang, C.H., Park, J., Pathania, D., Castro, C.M., Fasano, A., Weissleder, R., Lee, H., 2017. *ACS Nano* 11, 10062–10069.
- Lin, Y., Huang, C., Chang, H., 2011. *Analyst* 136, 863–871.
- Liu, D., Wang, Z., Jiang, X., 2011a. *Nanoscale* 3, 1421–1433.
- Liu, J., Lu, Y., 2007. *Angew. Chem. Int. Ed.* 46, 7587–7590.
- Liu, X., Miao, L., Jiang, X., Ma, Y., Fan, Q., Huang, W., 2011b. *Chin. J. Chem.* 29, 1031–1035.
- Lu, Z., O'Dell, D., Srinivasan, B., Rey, E., Wang, R., Vemulapati, S., Mehta, S., Erickson, D., 2017. *Proc. Natl. Acad. Sci. USA* 114, 13513–13518.
- Ludwig, S.K.J., Zhu, H., Phillips, S., Shiledar, A., Feng, S., Tseng, D., van Ginkel, L.A., Nielsen, M.W., Ozcan, A., 2014. *Anal. Bioanal. Chem.* 406, 6857–6866.
- Meng, X., Huang, H., Yan, K., Tian, X., Yu, W., Cui, H., Kong, Y., Xue, L., Liu, C., Wang, S., 2017. *Lab Chip* 17, 104–109.
- Mertens, S.F.L., Gara, M., Sologubenko, A.S., Mayer, J., Szidat, S., Krämer, K.W., Jacob, T., Schiffrin, D.J., Wandlowski, T., 2011. *Adv. Funct. Mater.* 21, 3259–3267.
- Miao, P., Liu, L., Li, Y., Li, G., 2009. *Electrochem. Commun.* 11, 1904–1907.
- Nolan, E.M., Lippard, S.J., 2008. *Chem. Rev.* 108, 3443–3480.
- Ono, A., Togashi, H., 2004. *Angew. Chem. Int. Ed.* 43, 4300–4302.
- Park, H., Hwang, S., Kim, K., 2012. *Electrochem. Commun.* 24, 100–103.
- Saidura, M.R., Aziza, A.R.A., Basirun, W.J., 2017. *Biosens. Bioelectron.* 90, 125–139.
- Santos, V.C.G., Grassi, M.T., Campos, M.S., Zamora, P.G.P., Abate, G., 2012. *Analyst* 137, 4458–4463.
- Shah, A.Q., Kazi, T.G., Baig, J.A., Afridi, H.I., Kandhro, G.A., Khan, S., Kolachi, N.F., Wadhwa, S.K., 2010. *Food Chem. Toxicol.* 48, 1550–1554.
- Sugiyama, H., Adachi, N., Kawauchi, S., Kozasa, T., Katayama, T., Torigoe, H., Ono, A., Tamura, Y., 2005. *Nucleic Acids Symp. Ser.* 49, 215–216.
- Tanaka, Y., Oda, S., Yamaguchi, H., Kondo, Y., Kojima, C., Ono, A., 2007. *J. Am. Chem. Soc.* 129, 244–245.
- Thompson, R.B., 2005. *Fluorescence Sensors and Biosensors*, 1st ed. CRC Press, Boca Raton.
- Vashist, S.K., Lippa, P.B., Yeo, L.Y., Ozcan, A., Luong, J.H.T., 2015. *Trends Biotechnol.* 33, 692–705.
- Wang, R., Zhou, X., Shi, H., Luo, Y., 2016. *Biosens. Bioelectron.* 78, 418–422.
- Wu, D., Wang, Y., Zhang, Y., Ma, H., Pang, X., Hu, L., Du, B., Wei, Q., 2016. *Biosens. Bioelectron.* 82, 9–13.
- Wei, Q., Nagi, R., Sadeghi, K., Feng, S., Yan, E., Ki, S.J., Caire, R., Tseng, D., Ozcan, A., 2014. *ACS Nano* 8, 1121–1129.
- Wei, Q., Qi, H., Luo, W., Tseng, D., Ki, S.J., Wan, Z., Gorocs, Z., Bentolila, L.A., Wu, T., Sun, R., Ozcan, A., 2013. *ACS Nano* 7, 9147–9155.
- Wu, S., Zhang, B., Wang, F., Mi, Z., Sun, J., 2018. *Biosens. Bioelectron.* 104, 145–151.
- Xu, A., Chao, L., Xiao, H., Sui, Y., Liu, J., Xie, Q., Yao, S., 2018. *Biosens. Bioelectron.* 104, 95–101.
- Yang, J., Yang, T., Wang, X., Chen, M., Yu, Y., Wang, J., 2018. *Anal. Chem.* 90, 6945–6951.
- Yang, K., Zeng, M., Hu, X., Guo, B., Zhou, J., 2014. *Analyst* 139, 4445–4448.
- Yuan, T., Liu, Z., Hu, L., Zhang, L., Xu, G., 2011. *Chem. Commun.* 47, 11951–11953.
- Yue, S., Zhao, T., Bi, S., Zhang, Z., 2017. *Biosens. Bioelectron.* 98, 234–239.
- Zeng, G., Zhang, C., Huang, D., Lai, C., Tang, L., Zhou, Y., Xu, P., Wang, H., Qin, L., Cheng, M., 2017. *Biosens. Bioelectron.* 90, 542–548.
- Zhang, J., Huang, W., Zeng, A., Luo, H., Li, N., 2015. *Biosens. Bioelectron.* 64, 597–604.
- Zhu, H., Sencan, I., Wong, J., Dimitrov, St, Tseng, D., Nagashima, K., Ozcan, A., 2013. *Lab. Chip* 13, 1282–1288.